Investigation and Wind Tunnel Test on Gust Load Alleviation for a Flying Wing

Yuntao Xu[1,2(✉)], Yi Liu[2], Zhigang Wu[1], and Chao Yang[1]

[1] School of Aeronautic Science and Engineering, Beihang University, Beijing 100083, People's Republic of China
18001033551@163.com

[2] Beijing Institute of Mechanical and Electrical Engineering, Beijing 100074, People's Republic of China

Abstract. Based on the latest developments in gust alleviation technology, this paper studies and establishes the modeling methods, control scheme design and practical alleviation methods for gust alleviation techniques. The effectiveness of the modeling method and the gust alleviation control scheme was verified by wind tunnel tests.

Keywords: wind tunnel test · gust load alleviation · flying wing

1 Introduction

The aerodynamic forces and moments generated by the aircraft passing through the gust zone will cause additional load to the aircraft. This additional load will reduce the flight quality of the aircraft, causing the aircraft to withstand large structural dynamic loads, resulting in reduced fatigue life of components such as wings and the body.

With the continuous development of aviation science and technology, the design of aircraft is moving toward the trend of low structural weight and flexibility, which makes the impact of gusts on the aircraft more complicated. This complexity is reflected in the fact that the gusts not only cause the rigid body motion of the aircraft, but also increase the normal overload, and at the same time, due to the elasticity of the aircraft body, it will cause structural elastic vibration of the aircraft. The modal vibration of the aircraft structure caused by gust excitation is more serious for the flying wing layout.

Based on the above research background, the purpose of this paper is to model the gust response of elastic wing and elastic aircraft for the flying-wing UAV, and to explore the elastic gust alleviation control method and wind tunnel test method.

2 Model and Numerical Method

2.1 Flying Wing Model

The wind tunnel test model is shown in Fig. 1. It is mainly assembled with four parts: metal skeleton and support frame, pneumatic enclosure and rudder surface, steering gear, sensor and support system. The actual length of the model is 1.8 m and the total weight

Chinese Society of Aeronautics and Astronautics (Ed.): CASTC 2023, LNME, pp. 550–558, 2024.
https://doi.org/10.1007/978-981-99-8867-9_52

is nearly 12 kg. The model is equipped with three rudder surfaces to implement gust alleviation active control, which is clearly the first, second and third rudder surfaces from the inside out. No. 2 rudder surface is used for height maintenance control, while gust alleviation control is mainly carried out through No. 3 rudder surface. There are five types of sensors in the model to measure the corresponding state of the model. In addition, the model is attached to a support system that provides both degrees of freedom of up and down and pitch stiffness.

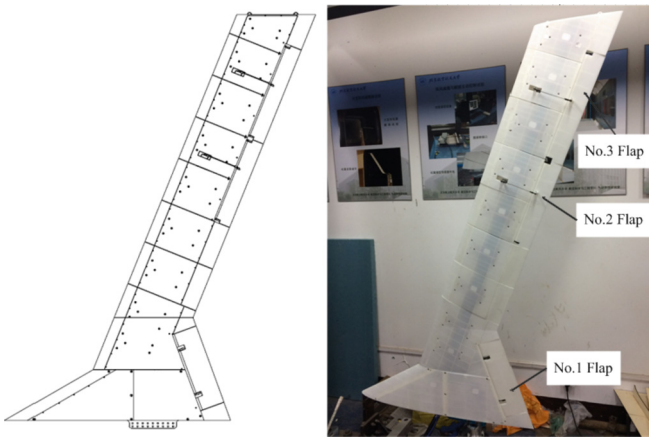

Fig. 1. Model design and actual appearance

2.2 Finite Element Model

According to the above structural form, a NASTRAN finite element model as shown in Fig. 2 is established. The structural characteristics of the metal skeleton and the support system shaft are simulated by the BEAM elements, and the remaining components are simplified to the CONM2 elements and connected to the BEAM elements through the RBE2 or RBAR elements. The mass of each rudder surface is represented by the CONM2 elements and is connected by the RBE2 elements to a "rigid" BEAM elements arranged on the axis of rotation with a zero material density. Similar rigid elements are also attached to the BEAM elements representing the skeleton to facilitate aeroelastic interpolation. In addition, the PLOTEL elements are used to outline the aerodynamic shape of the model.

The vibration characteristics of the model under the condition of root fixation are shown in Fig. 3. The theoretical and measured values of the first four natural modal frequencies are shown in Table 1. The result shows that the theoretical value of the natural frequency of the model is in good agreement with the measured value, and the simulation of the stiffness and mass of the physical model by the finite element model is reasonable.

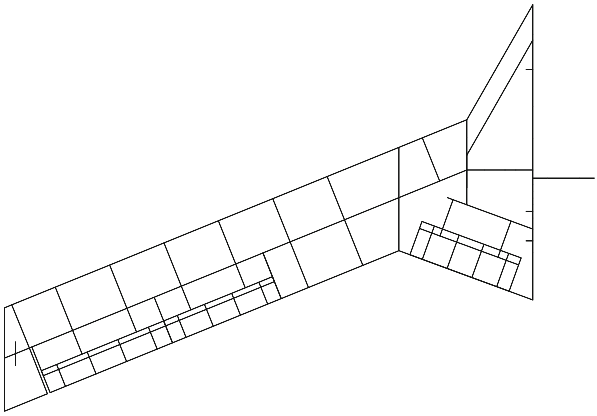

Fig. 2. Finite element model of the flying wing

Table 1. First four-order modal under the condition of root fixation

Modal name	Theoretical frequency/Hz	Measured frequency/Hz
First vertical bending mode	2.36	2.33
First horizontal bending mode	4.65	4.50
Second vertical bending mode	16.02	14.25
First vertical twist mode	25.15	23.43

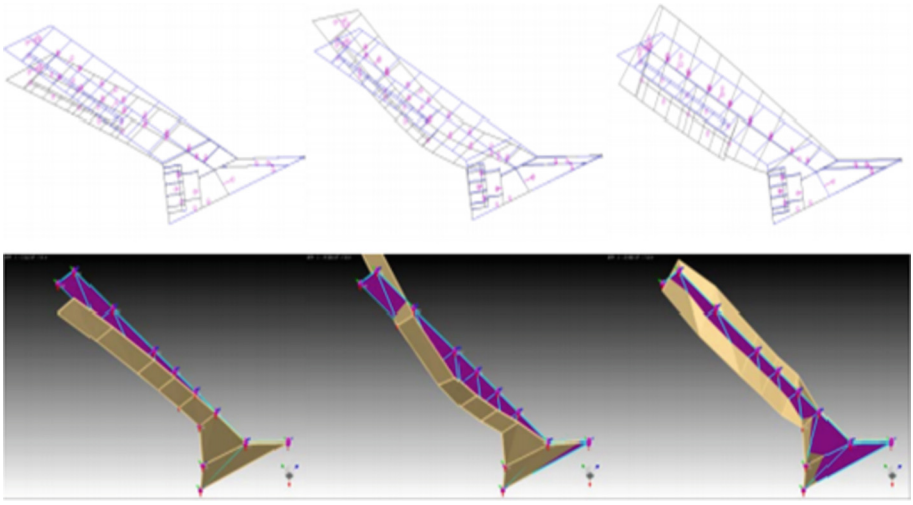

Fig. 3. First three-order modal array under the condition of root fixation

2.3 Gust Generator

The gust generator swings at different frequencies to produce a sinusoidal gust. The gust generator adopts two blades, and is driven by the driving device to reciprocate around its own rotating shaft according to a given frequency and amplitude to achieve the purpose of generating a desired sinusoidal gust in the flow field of the test section. The gust generator is shown in Fig. 4.

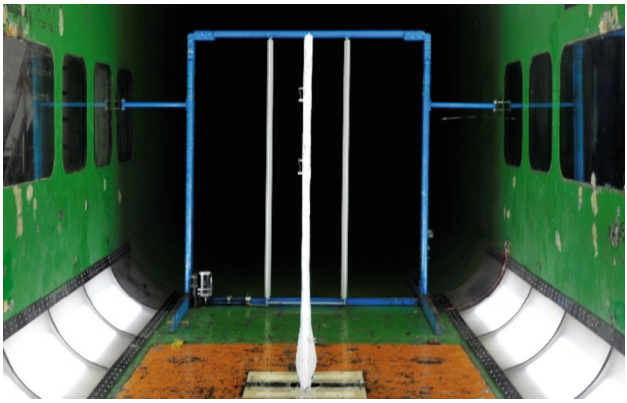

Fig. 4. Gust generator placed in the wind tunnel

2.4 Active Control Law Design

The closed-loop aeroservoelastic system for the wind tunnel test is shown in Fig. 5. The input is a sin type gust generated by the gust generator. The response signal for feedback control is input to the design control law. The control law can be divided into two parts according to the purpose: One part is used for height hold control, so that the rigid body motion of the open loop system remains stable; the other part is used for gust alleviation control, which reduces the gust response of the open loop system.

2.5 Simulations

Establish the structural dynamic equations according to Language equations. The is the grid degree of freedoms

$$\mathbf{M}\ddot{x} + \mathbf{D}\dot{x} + \mathbf{K}x = \mathbf{f} \tag{1}$$

In order to reduce the direct numerical calculations, the equations above can be written in modal space.

$$\mathbf{\Phi}^T\mathbf{M}\Phi\ddot{x} + \mathbf{\Phi}^T\mathbf{D}\Phi\dot{x} + \mathbf{\Phi}^T\mathbf{K}\Phi x = \mathbf{\Phi}^T\mathbf{f} \tag{2}$$

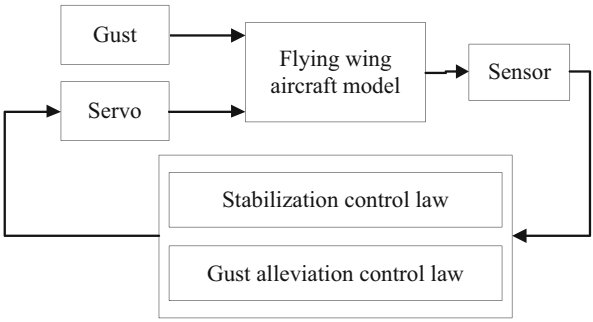

Fig. 5. Closed-loop aeroservoelastic system for wind tunnel test

Which $\mathbf{\Phi}^T\mathbf{M}\Phi = \mathbf{I}$, $\mathbf{\Phi}^T\mathbf{K}\Phi = diag(\mathbf{k})$. Assume that the damping is proportion to the mass and stiffness, structural dynamic equations can be rewritten as:

$$\begin{bmatrix} \mathbf{M}_{RR} & \mathbf{M}_{RE} \\ \mathbf{M}_{ER} & \mathbf{M}_{EE} \end{bmatrix} \ddot{\boldsymbol{x}} + \begin{bmatrix} \mathbf{0} & \mathbf{0} \\ \mathbf{0} & \mathbf{D}_E \end{bmatrix} \dot{\mathbf{x}} + \begin{bmatrix} \mathbf{0} & \mathbf{0} \\ \mathbf{0} & \mathbf{K}_E \end{bmatrix} \mathbf{x} = \begin{bmatrix} \mathbf{f}_R \\ \mathbf{f}_E \end{bmatrix} \tag{3}$$

The right-hand of the equations is aerodynamic forces, which can be obtained by double-lattice method in frequency domain.

$$\begin{bmatrix} \mathbf{f}_R \\ \mathbf{f}_E \end{bmatrix} = q_\infty \big[Q_{hh}(ik)\big]\{\xi\} + q_\infty \big[Q_{hc}(ik)\big]\{\delta\} \tag{4}$$

The general unsteady aerodynamics can be expressed as:

$$\begin{aligned} [\tilde{Q}(s)] = \big[Q_{hh}(s), Q_{hc}(s)\big] &= [A_0] + \frac{L}{V}[A_1]s \\ &+ \frac{L^2}{V^2}[A_2]s^2 + [D]\left[s[I] - \frac{V}{L}[R]\right]^{-1}[E]s \end{aligned} \tag{5}$$

The frequency domain aerodynamic force can not be used in time domain simulation, so the aerodynamic forces should be spread over all complex plane with rational function fitting methods. R_i is lagging roots

$$R_i = -1.7k_{\max}\left(\frac{i}{N_{lag}+1}\right)^2, i = 1, 2, ..N_{lag} \tag{6}$$

Use minimum state method to fitting the aerodynamic forces and separate it into real part and image part

$$\mathrm{Re}[\tilde{Q}(ik)] \approx [A_0] - k^2[A_2] + k^2[D]\left[k^2[I] + [R]^2\right]^{-1}[E] \tag{7}$$

$$\mathrm{Im}[\tilde{Q}(ik)] \approx k[A_1] - k[D]\left[k^2[I] + [R]^2\right]^{-1}[R][E] \tag{8}$$

The fitting errors can be evaluated by equations below.

$$\varepsilon_{ijl} = \left|\tilde{Q}_{ij}(ik_l) - Q_{ij}(ik_l)\right| W_{ijl} \tag{9}$$

Then the state equations for gust can be established as:

$$\left\{\dot{X}_{ae}\right\} = [A_{ae}]\{X_{ae}\} + [B_{ae}]\{U_{ae}\} + [B_{aw}]\left\{\overline{w}_g\right\} \tag{10}$$

$$[A_{ae}] = \begin{bmatrix} [0] & [I] & [0] \\ -[\overline{M}]^{-1}\left[[K_{hh}] - q_\infty\left[A_{hh_0}\right]\right] & -[\overline{M}]^{-1}\left[[C_{hh}] - q_\infty \frac{L}{V}\left[A_{hh_1}\right]\right] & q_\infty[\overline{M}]^{-1}\left[D^*\right] \\ [0] & [E_h] & \frac{V}{L}\left[R^*\right] \end{bmatrix} \tag{11}$$

$$[B_{ae}] = \begin{bmatrix} [0] & [0] & [0] \\ q_\infty[\overline{M}]^{-1}\left[A_{hc_0}\right] & q_\infty \frac{L}{V}[\overline{M}]^{-1}\left[A_{hc_1}\right] & -[\overline{M}]^{-1}\left[[M_{hc}] - \frac{q_\infty L^2}{V^2}\left[A_{hc_2}\right]\right] \\ [0] & [E_c] & [0] \end{bmatrix} \tag{12}$$

$$[B_{aw}] = \begin{bmatrix} [0] & [0] \\ q_\infty[\overline{M}]^{-1}\left[A_{hg_0}\right], & q_\infty \frac{L}{V}[\overline{M}]^{-1}\left[A_{hg_1}\right] \\ [0] & \left[E_g\right] \end{bmatrix} \tag{13}$$

According to the stablished theoretical gust response analysis model, the simulated flying wing gust response results are presented below. The biggest responses amplitude of inner force are located at the wing first bend model while the torsion response is higher which is near to the twist mode (Fig. 6).

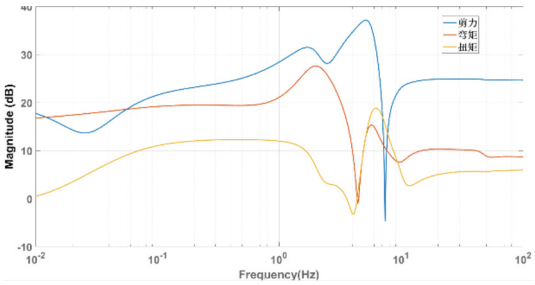

Fig. 6. Shear, bend moment and torsion at wing root under different gust frequency

3 Results and Discussion

Validation studies are first performed on wind tunnel testing to make sure that the present model is applicable for the problem of interest.

3.1 Model in the Wind Tunnel

The test model, the support system, and the installation of the gust generator in the wind tunnel are shown in Fig. 23. The gust generator is installed 3 m in front of the wind tunnel model. Under the motor drive, the gust generator is deflected by two NACA0020 wing segments with a length of 2 m and a chord length of 0.2 m. The gust frequency is in the range of 1 Hz to 5 Hz.

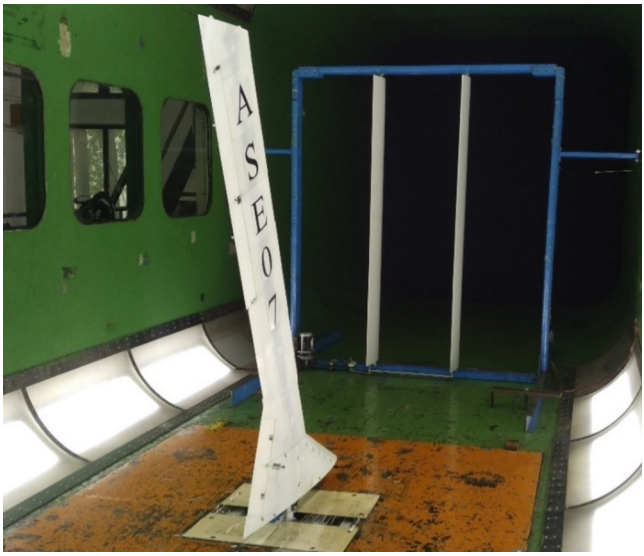

Fig. 7. Model in the wind tunnel

3.2 Open Loop Gust Response

When the wind speed is 20 m/s and the gust frequency is 1.2 Hz, the wingtip acceleration is shown in Fig. 7. It can be seen that the simulation and wind tunnel test are in good agreement in the open loop case.

3.3 Closed Loop Gust Response

Wing tip acceleration response at different gust frequencies and different wind speeds is shown in Fig. 8. The results show that the gust alleviation control law designed in the low frequency band has a significant effect, and both the wing tip acceleration and the wing root bending moment have obvious alleviation effects. Because in the low frequency band, that is, about 1 Hz, the response of the model is mainly concentrated on the pitch modal frequency of the model. Using the angle and angular rate signals as feedback, the pitch motion of the model can be effectively suppressed and the effect is obvious. At high frequencies, the effect of the gust alleviation control law is not obvious, and

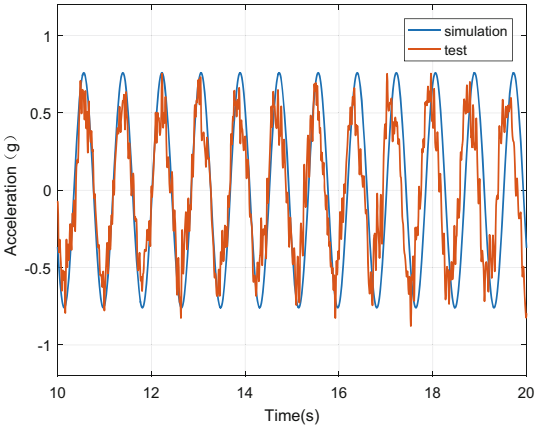

Fig. 8. Wing tip leading edge acceleration at wind speed 20 m/s, gust frequency 1.2 Hz

the response is even increased. Because at high frequencies, the response of the model is concentrated at one of its bending elastic frequencies. However, the feedback of the wingtip acceleration signal is not added in the design of the gust alleviation control law, that is, the control law does not slow down the elastic frequency of the model (Fig. 9).

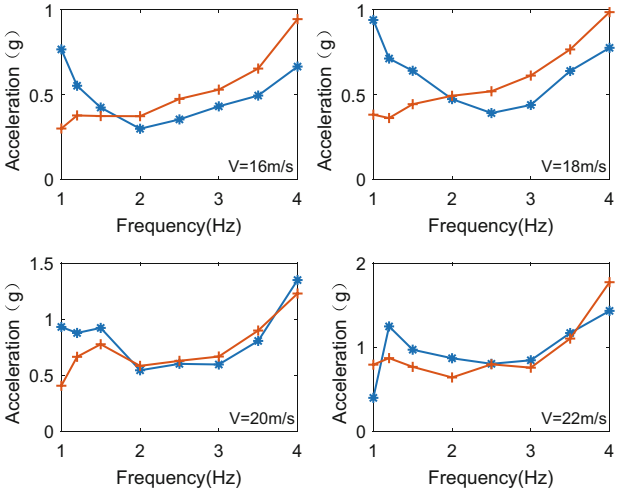

Fig. 9. Wing tip acceleration response at different gust frequencies and different wind speeds (blue: open loop; red: closed loop) (Color figure online)

4 Conclusions

The gust response is calculated by the time domain gust response modeling method. The results show that the gust alleviation control scheme can reduce the wingtip acceleration and wing root moment response of the model under certain wind speed and certain gust frequency.

References

1. Fuller, J.R.: Evolution of airplane gust loads design requirements. J. Aircr. **32**(2), 235–246 (1995)
2. Murrow, H.N., Pratt, K.G., Houbolt, J.C.: NACA/NASA Research Related to Evolution of U.S. Gust Design Criteria. AIAA-1989-1373-CP. AIAA, Reston (1989)
3. Xie, C., Wang, L., Yang, C.: Static aeroelastic analysis of very flexible wings based on non-planar vortex lattice method. Chin. J. Aeronaut. **26**(3), 514–521 (2013)
4. Su, W., Cesnik, C.E.S.: Dynamic response of highly flexible flying wings. AIAA J. **49**(2), 324–339 (2011)
5. Vartio, E.J., Shaw, E.E., Vetter, T.: Gust load allevia-tion flight control system design for a SensorCraft vehicle. In: 26th AIAA Applied Aerodynamics Confer-ence, Honolulu, Hawaii, 18–21 August 2008, AIAA-2008-7192. AIAA, Reston (2008)
6. Dillsaver, M.J., Cesnik, C.E.S.: Gust load alleviation control for very flexible aircraft. In: 52th AIAA Atmospheric Flight Mechanics Conference, Portland, Oregon, 8–11 August 2011 (2011)
7. Scott, R.C., Vetter, T.K., Penning, K.B., et al.: Aeroservoelastic Testing of Free Flying Wind Tunnel Models, Part 1: a Sidewall Supported Semispan Model Tested for Gust Load Alleviation and Flutter Suppression, NASA/TP-2013-218051. NASA Langley Research Center, Hampton (2013)
8. Tang, D., Grasch, A.: Gust response for flexibly suspended high-aspect ratio wings. AIAA J. **48**(10), 2430–2444 (2010)
9. Dillsaver, M.J., Cesnik, C.E.S.: Gust response sensitivity characteristics of very flexible aircraft. In: 53th AIAA Atmospheric Flight Mechanics Conference, Minneapolis, Minnesota, 13–16 August 2012 (2012)
10. Shi, Y., Wan, Z.Q., Wu, Z.G., et al.: Gust response analysis and verification of elastic aircraft based on nonlinear aerodynamic reduced-order model. Acta Aeronaut. Astronaut. Sin. **43**(1), 125474 (2022). (in Chinese)
11. Wang, Y., Li, F., Ronch, A.D.: Flight Testing Adaptive Feedback/Feedforward Controller for Gust Loads Alleviation on a Flexible Aircraft. AIAA-2016-3100. AIAA, Reston (2016)
12. Zhang, J.H.: Study on Gust Alleviation for Flying Wing Aircraft, pp. 25–27. Beihang University, Bejing (2020)
13. Liu, X., Sun, Q.: Gust load alleviation with robust control for a flexible wing. Shock. Vib. **2016**, 1060574 (2016)
14. Yang, X.M., Liu, N., Guo, C.P.: A survey of aeroelastic wing tunnel test technology of flight vehicles. Acta Aerodyn. Sin. **36**(6), 995–1008 (2018)
15. An, C., Xie, C.C., Meng, Y.: Wind tunnel test and gust load alleviation of flexible wing including geometric nonlinearity with servo control. In: 2018 AIAA/ASCE/AHS/ASC structures. Structural Dynamics, and Materials Conference. Reston (2018)
16. Nazeer, N., Wang, X.R.: Sensing, actuation, and control of the SmartX prototype morphing wing in the wind tunnel. Actuators **10**(6), 107 (2021)